LRP 432/91 August 1991

# NON-LOCAL EFFECTS OF ALPHA PARTICLES ON SECOND-HARMONIC HEATING

O. Sauter & J. Vaclavik

# Non-local effects of alpha particles on second-harmonic heating

O. Sauter and J. Vaclavik

Centre de Recherches en Physique des Plasmas
Association Euratom - Confédération Suisse
Ecole Polytechnique Fédérale de Lausanne
21, Av. des Bains - CH-1007 Lausanne - Switzerland

Abstract

A model based on the linearized Vlasov-Maxwell equations, taking into account the non-local interactions of particles due to their finite Larmor radii, has been developed. Assuming an inhomogeneous 1-D slab plasma, Maxwellian equilibrium distribution functions and $k_y=0$, it leads to a system of one first-order and two second-order integro-differential equations for $E_x$ and $E_y$, $E_z$ respectively. These equations are valid for arbitrary value of $k_\perp\rho_\sigma$, where $k_\perp$ is the perpendicular wavenumber and $\rho_\sigma$ the Larmor radius of species $\sigma$. Therefore, the code SEMAL [4], solving these equations, is well appropriate for studying the effects of alpha particles on the ion cyclotron range of frequency (ICRF) heating. These effects are shown to be much less significant for heating at the second harmonic of deuterium than expected from local models. Other heating scenarii of deuterium as well as the influence of $k_z$, $T_\alpha$, non-Maxwellian distribution functions and $n_\alpha/n_e$ are also investigated. The results indicate under which conditions the power absorption by alpha particles start to dominate and, therefore, degrade the heating efficiency.

# 1. INTRODUCTION

In present days large tokamaks, ICRF heating has proved to be a very efficient heating scenario and it may be one of the main heating method for future thermonuclear fusion experiments. An important question is the influence of high-energetic alpha particles on the heating efficiency. Hellsten et al [1] were first to draw the attention to the problem of strong alpha particle absorption during various ICRH scenarii. Using a local model valid up to second order in $k_\perp \rho_\sigma$, they showed that, for second-harmonic of deuterium scenarii, all the power can be absorbed by the alphas near the edge for concentrations $n_\alpha/n_e$ larger than 1%. But as $k_\perp \rho_\alpha$ was larger than one, the model was not valid for the alphas and another model is needed to have better quantitative results. Kay et al. [2] investigated this effect using a simplified mode-conversion equation valid around ion-cyclotron resonances and taking the contribution of alphas as a small perturbation to the basic wave. In this way they could evaluate the contribution of alphas to all orders in $k_\perp \rho_\alpha$ and compare the power absorbed by the alphas ($P_\alpha$) and deuterium ($P_D$) at the second harmonic. They found that the alpha particles absorbed much more power than deuterium for $k_\parallel R_0 < 4$ and about the same amount for $k_\parallel R_0 \geq 4$. However, this model is not yet sufficient for simulating a complete heating scenario. In particular, one needs to know if the wave is completely absorbed by the alphas in the outer part of the plasma, that is in between resonances, before it reaches the resonance layer of deuterium.

In order to answer this question, the equations need to be solved throughout the whole plasma. Two methods have been used : ray-tracing [3] and global wave [4]. The extension of ray-tracing codes is

straightforward as one only needs to solve the dispersion relation valid to all orders in $k_\perp \rho_\sigma$. Using such a code, Van Eester et al. [3] found, for NET-ITER plasma parameters, that $P_\alpha$ is of the same order as $P_D$ for $n_\alpha/n_e \cong 1\%$ and larger for larger concentrations. This confirms that $P_\alpha$ was overestimated by the local model used in [1]. However, in the heating scenario considered by Hellsten et al. [1], the fourth harmonic of tritium lies near the edge (x = 1m) as can be seen in Fig. 1. Therefore, one needs the global wave solution of the linearized Maxwell-Vlasov equations to obtain reliable quantitative results. The extension of local global-wave models to non-local ones leads to solving a system of second-order integro-differential equations. It needs a rather large amount of computing time, which is why we have developed our model in a 1-D slab geometry. It was first solved using the electrostatic approximation [5] and then extended to the full electromagnetic wave problem [4]. The code SEMAL is now appropriate for studying Bernstein waves, higher-harmonic heating and/or alpha particles effects. In Section II we shall briefly derive the equations for the three components of the electric field and the formula for the power absorption. Then, we shall present our results in two subsections : III.1 - comparison with the results obtained with a local model by Hellsten et al. [1]; III.2 - influence of $k_z$, $T_\alpha$, $n_\alpha/n_e$ and non-Maxwellian distribution functions. Finally, a summary of our results and of the main constraints on the heating scenarii will be presented in Section IV.

# 2. PHYSICAL MODEL

## 2.1 Integro-differential equations for $\underline{E}$

The linear wave-particle interaction in hot plasmas can be described by the linearized Vlasov-Maxwell system of equations. As mentioned before, we shall restrict ourselves to 1-D slab plasma, but allow for arbitrary inhomogeneous density and temperature profiles, and for a slowly varying magnetic field. The aim of this new model is to keep the equations valid to all orders in Larmor radii while solving for the electric field in the whole plasma at once, together with the boundary conditions. The plasma is assumed to be surrounded by vacuum in which there is, on the right-hand side of the plasma, an infinitely thin sheet antenna current in the (y, z) plane. The equilibrium magnetic field $B_0$ is along the z-direction and the inhomogeneity along x. We shall neglect $k_y$ in the dielectric response of the plasma and assume Maxwellian equilibrium distribution functions.

This global wave model leads to solving second-order integro-differential equations. Thus, the solution at one point is influenced by the whole plasma, which is why this model is called non-local. In practice, as will be seen below, only the points distant up to four or five Larmor radii contribute. The other advantage of this model is that it can apply to frequencies larger than the second harmonic of the cyclotron frequency. A code SEAL, solving these equations in the electrostatic approximation to all orders in Larmor radii has already been developed and was able to simulate quite well an experiment involving Bernstein waves [5] The

procedure for treating the electromagnetic case is the same as in [5] and has been presented in [4]. Therefore, we shall only briefly discuss it here.

First we linearize the Vlasov and Maxwell equations and Fourier transform them. Then we solve for the perturbed distribution function $f_\sigma^{(1)}(\underline{k}, \underline{v}, \omega)$, which involves a convolution between the inhomogeneous equilibrium distribution function $f_\sigma^{(0)}$ and the electric field. Note that by Fourier transforming $f_\sigma^{(0)}$, the perpendicular precession of the particles is uncoupled from the motion of guiding centers and only the density and temperature profiles of the guiding centers are needed.

Then, the current contribution in Maxwell's equations is calculated using $f_\sigma^{(1)}(\underline{k}, \underline{v}, \omega)$. In order to be able to invert the Fourier transform of the resulting equations, we assume $k_y = 0$ in the current contribution and Maxwellian equilibrium distribution function of the form :

$$f_\sigma^{(0)}(v_\perp, v_{//}, \mathbf{k}_\perp) = f_\sigma^{(0)}(v_\perp, v_{//}, k_x) = \frac{1}{2\pi^{5/2}} \int dx'' \, \frac{n_\sigma(x'')}{v_{T\sigma}^3(x'')} \exp\left\{ - \frac{v_\perp^2 + v_{//}^2}{v_{T\sigma}^2(x'')} \right\} e^{-i k_x x''},$$

where $v_{T\sigma}^2 = 2T_\sigma / m_\sigma$, and $n_\sigma$ and $T_\sigma$ are the density and temperature of the guiding centers respectively. We shall use throughout this paper the variable x'' for the inhomogeneity. Note also that we have checked with our local model that $k_y$ has very little influence in ICRF heating, especially at higher harmonics. We have also used the following integral representation of the Bessel function $I_n$ :

$$I_n(k_x^2\rho_\sigma^2) = \frac{1}{\pi}\int_0^\pi e^{k_x^2\rho_\sigma^2\cos\theta}\cos(n\theta)\,d\theta\ .$$

In this way, we are able to integrate exactly over $k_x$ and $\underline{v}$, and we obtain the following system of equations for the three components of the electric field [4] :

$$\nabla\wedge\nabla\wedge\mathbf{E}(x) - \frac{\omega^2}{c^2}\mathbf{E}(x) - i\mu_0\omega(\underline{\underline{\sigma}}\mathbf{E})(x) = 0, \qquad (1)$$

with

$$(\underline{\underline{\sigma}}\mathbf{E})(x) \equiv \sum_{\sigma,n} -\frac{iq_\sigma^2}{2\pi m_\sigma k_z}\int dx''\,dx'\int_0^\pi d\theta\,\frac{n_\sigma(x'')}{v_{T\sigma}(x'')}\exp\left\{-\frac{(x-x')^2(1-\cos\theta)}{2\rho_\sigma^2(x'')\sin^2\theta}\right\}$$
$$\exp\left\{-\frac{(x''-\frac{x+x'}{2})^2(1+\cos\theta)}{\rho_\sigma^2(x'')\sin^2\theta}\right\}\ \bar{\underline{\sigma}}(x,x',x'',\theta)\,\mathbf{E}(x')$$

$$\bar{\sigma}_{xx} = -\frac{nZ_n}{\pi\rho_\sigma^2}\sin n\theta\ ,$$

$$\bar{\sigma}_{yy} = -\frac{Z_n}{\pi\rho_\sigma^4}(x-x'')(x'-x'')\frac{\cos n\theta}{\sin\theta} - \frac{\sqrt{2\pi}k_z v_{T\sigma}}{\omega\rho_\sigma}\left(\frac{(x-x'')^2}{\rho_\sigma^2}-1\right)e^{\frac{(x-x'')^2}{2\rho_\sigma^2}}\delta(x-x')\,\delta(\theta-\frac{\pi}{2})\ ,$$

$$\bar{\sigma}_{zz} = -\frac{2}{\pi\rho_\sigma^2}\xi_n(1+\xi_n Z_n)\frac{\cos n\theta}{\sin\theta}\ ,$$

$$\bar{\sigma}_{xy} = \frac{iZ_n}{\pi\rho_\sigma^4}(x'-x'')\left[(x-x'')\cos\theta - (x'-x'')\right]\frac{\sin n\theta}{\sin^2\theta}\ ,$$

$$\bar{\sigma}_{yx} = -\frac{iZ_n}{\pi\rho_\sigma^4}(x-x'')\left[(x'-x'')\cos\theta - (x-x'')\right]\frac{\sin n\theta}{\sin^2\theta}\ ,$$

$$\bar{\sigma}_{xz} = -\frac{2i\omega_{c\sigma}}{\pi\rho_\sigma^2 v_{T\sigma}} \xi_n Z_n \left[(x-x'')\cos\theta - (x'-x'')\right] \frac{\sin n\theta}{\sin^2\theta},$$

$$\bar{\sigma}_{zx} = \frac{2i\omega_{c\sigma}}{\pi\rho_\sigma^2 v_{T\sigma}} \xi_n Z_n \left[(x'-x'')\cos\theta - (x-x'')\right] \frac{\sin n\theta}{\sin^2\theta},$$

$$\bar{\sigma}_{yz} = \frac{2\omega_{c\sigma}}{\pi\rho_\sigma^2 v_{T\sigma}} (1+\xi_n Z_n)\,(x-x'') \frac{\cos n\theta}{\sin\theta},$$

$$\bar{\sigma}_{zy} = \frac{2\omega_{c\sigma}}{\pi\rho_\sigma^2 v_{T\sigma}} (1+\xi_n Z_n)\,(x'-x'') \frac{\cos n\theta}{\sin\theta},$$

where $\omega_{c\sigma} = q_\sigma B_0/m_\sigma$ and $\xi_{n\sigma} = (\omega - n\omega_{c\sigma})/k_z v_{T\sigma}$ are the cyclotron frequency and the argument of the Fried-Conte dispersion function $Z_n$ [6], respectively, and $\rho_\sigma^2 = v_{T\sigma}^2/2\omega_{c\sigma}^2$. Equation (1) is a system of one first-order and two second-order integro-differential equations for $E_x$ and $E_y$, $E_z$ respectively. It is solved in the code SEMAL using a finite element method and Gaussian quadratures for the integrals. Due to the asymmetry between $E_x$ and $E_y$, $E_z$, we have used piece-wise constant basis functions for $E_x$ and linear for $E_y$, $E_z$, in order to avoid pollution problems [7].

One can see from Eq. (1) that the non-local interaction is limited in space by the terms :

$$\exp\left\{-\frac{(x-x')^2\,(1-\cos\theta)}{2\rho_\sigma^2(x'')\sin^2\theta}\right\}$$

and

$$\exp\left\{-\frac{\left(x''-\frac{x+x'}{2}\right)^2(1+\cos\theta)}{\rho_\sigma^2(x'')\sin^2\theta}\right\}$$

The maximum width of interactions is about 5-7 Larmor radii, that is about 35-50cm for alpha particles with $T_\alpha$ = 3.5MeV and $B_0$ = 2.71T. This shows why a non-local model is needed for the alpha particles.

## 2.2 Power absorption

The code SEMAL also computes the power deposition profile for each species. The local power absorption formula is obtained following the same procedure as in the electrostatic case [5]. With the help of a change of variables to the Lagrangian coordinates, we are able to eliminate the contribution of the particles streaming into and out the volume element considered. In this way, we obtain a positive definite local power absorption formula, assuming $k_y = 0$, valid to all orders in Larmor radii and for arbitrary inhomogeneous density and temperature profiles and a slowly varying magnetic field :

$$P_L(x) = \sum_{n,\sigma} \frac{2q_\sigma^2}{\pi^{5/2} m_\sigma |k_z|} \int dx'' \int_0^{\frac{\pi}{2}} d\theta \frac{n_\sigma(x'')\,\omega_{c\sigma}^4(x'')}{v_{T\sigma}^5(x'')} \exp\left\{-\frac{(x-x'')^2}{2\rho_\sigma^2 \cos^2\theta}\right\} \frac{|x-x''|^3}{\cos^4\theta}$$

$$e^{-\xi_{n\sigma}^2} \left| \int_0^\pi d\theta' \left[ E_x \sin\theta' \sin n\theta' + i \cos n\theta' \left(\cos\theta' E_y + \frac{(\omega - n\omega_{c\sigma})\cos\theta}{k_z \omega_{c\sigma} |x-x''|} E_z\right)\right] \right|^2 \quad (2)$$

with

$$\mathbf{E} = \mathbf{E}\left(x'' - \frac{|x-x''|}{\cos\theta} \cos\theta'\right).$$

This formula corrects the one published in [4], where a non-resonant term was erroneously added to this formula. Note that it is not any more $|E_+|$ or $|E_-|$ which contribute, but a rather complicated combination of

$E_x$, $E_y$ and $E_z$. However, the integrand of the $\theta'$ integration can be rewritten as follows:

$$\frac{1}{2}\left[\cos(n-1)\theta' E_+ - \cos(n+1)\theta' E_-\right] + i \cos n\theta' \frac{(\omega - n\omega_{c\sigma})\cos\theta}{k_z \omega_{c\sigma}|x-x''|} E_z$$

Thus, we see that it is nevertheless $E_+$ and $E_-$ which contribute to $\mathbf{E}_\perp$. We have checked that Eq. (2) reduces to the formula in [5] for the electrostatic approximation. We have also verified that we obtain the same power absorption for the electrons using Eq.(2) or an expanded formula [8], as $k_\perp \rho_e << 1$.

## 3. RESULTS

### 3.1 Comparison with the local model (Figures 2 and 3 of [1])

In this subsection, we shall compare the results of SEMAL with those of the code ISMENE for the cases presented in [1], Figs 2 and 3. The code ISMENE solves Eq. (1) expanded up to second order in Larmor radii, while taking into account the gradients of the equilibrium quantities [9]. Therefore, it is an even more complete local model than the one used in [1]. Nevertheless, it is limited to second harmonic as $I_n(x)$ is of the order of $O(x^n)$ and therefore harmonics $n \geq 3$ are neglected in this model.

We have taken the same standard plasma parameters as in [1] $x_{pr}=1.25$m, $B_0=2.71$T, $R_0=2.96$m, $B(x)=B_0R_0/(R_0+x)$, $k_z=5\text{m}^{-1}$, $k_y=0$, $n_D=n_T=0.5\cdot10^{20}\text{m}^{-3}$, $n_e=10^{20}\text{m}^{-3}$, $T_D=T_T=T_e=5$keV. The profiles are proportional to $(1 - 0.95(x/x_{pr})^2)^\gamma$, with $\gamma=1$ for the density and $\gamma=2$ for the

temperature. Throughout this paper we shall fix $n_e=10^{20}m^{-3}$ and calculate the ion concentrations such as to satisfy the neutrality condition while keeping $n_D = n_T$. The alpha density profile is also parabolic, but the temperature is homogeneous if not otherwise stated.

The full hot-plasma dispersion relation, valid to all orders in Larmor radii, is shown in Fig. 1 for the standard parameters with $n_\alpha/n_e$ = 1%. Note that harmonics up to n=20 where needed to resolve correctly the Bernstein wave near the resonances. Two cyclotron resonances occur inside the plasma, at x=0 and x=1m. At x=0, we have $\omega=2\omega_{cD}=2\omega_{c\alpha}=3\omega_{cT}$, and at x=1m, $\omega=4\omega_{cT}$. The wavelength of the fast wave is about 10 cm throughout the plasma and between 1mm and 1cm for the Bernstein wave. Note that the Bernstein wave can be excited directly from the plasma edge and it connects to the branch below $4\omega_{cT}$. Note also that, above second-harmonic of deuterium, the fast and Bernstein wave branches connect.

The effect of alpha particle concentrations from $n_\alpha/n_e$=0 to 1% is shown in Fig. 2 for the local and non-local models with $\omega=2\omega_{CD}$ at the center. The total integrated power absorption profile, defined as

$$\overline{P}_L(x) \equiv \sum_\sigma \overline{P}_{L\sigma}(x) \equiv \sum_\sigma \int_{x_{pr}}^{x} dx' P_{L\sigma}(x'),$$

where $P_{L\sigma}(x)$ is the power absorption of species $\sigma$, is plotted versus x. We see that there is a great discrepancy between the two models. For $n_\alpha/n_e$=1%, the local model predicts that 100% is absorbed by the alphas and none by the deuterium, while the non-local model gives 44% and 31% respectively. This difference can be explained by examining the local

power absorption formula. For small $k_\perp^2\rho_\sigma^2$, $P_L(x)$ (Eq. (2)) is proportional to $k_\perp^2\rho_\sigma^2$, but inversely for large $k_\perp^2\rho_\sigma^2$. Therefore, the power absorbed by the alphas is overestimated by the local model, as already mentioned in [1], and is sufficiently high to absorb the wave completely before it reaches the cyclotron resonance at the center (Fig. 2a). On the other hand, with the non-local model, Fig. 2b, the wave reaches the center and much more power is absorbed by the deuterium. This is clearly seen in Fig. 3, where we compare the real part of $E_X$ obtained in both models with $n_\alpha/n_e$=1%. With the local model, ISMENE, the wave is completely absorbed already at x=50 cm, whereas with the non-local model, it reaches the cyclotron resonance (x=0). However, another effect can compensate this, which is absorption at harmonics lying outside the plasma. For example, in the case considered, $\omega/\omega_{cD}$=2.7 at the plasma edge. Therefore no power can be absorbed by the deuterium at the third harmonic, whereas the alphas absorb as much power at the third harmonic (21.5% of total) as at the second harmonic (22.5%), due to their broad resonance layer. Note also that the Bernstein wave, excited at the plasma edge, appears on $E_X$, but it does not deposit much energy except a little to electrons.

The limit to the second harmonic is in fact one of the main drawbacks of the local model for such scenarii. This is shown in Fig. 4, where different scenarii at $\omega=2\omega_{cH}$, $2\omega_c{}^3He$, $2\omega_{cD}$ and $2\omega_{cT}$, are compared. They all have an alpha concentration of 1% and in the first two cases, hydrogen or $^3He$ has been added with $n_H/n_e = n^3{}_{He}/n_e = 20\%$. With ISMENE, the scenario tuned to the second harmonic of H is found to be much better than the others, whereas it is the opposite with SEMAL. This difference is essentially due to higher harmonic heating. Indeed, as $2\omega_{cH} = 4\omega_{c\alpha}$, then resonances at the fourth to sixth harmonic of $\omega_{c\alpha}$ occur in

the plasma and absorb most of the energy. These resonances are neglected in the local model. Moreover, if the frequency is higher, the distance between two successive resonances is shorter and the number of cyclotron resonances between the center and the edge of the plasma is increased. As an example, we show in Fig. 5 the power absorption density of the alphas for the case with hydrogen. We see that strong off-center power absorption occurs at the 5th (39%) and 6th (13%) harmonic compared with central absorption at the n=4 (11%). In this case, $P_\alpha/P_{tot}$=63% and $P_H/P_{tot}$=35%.

### 3.2 Influence of $T_\alpha$, $k_z$, $n_\alpha/ne$ and the type of distribution function

We shall discuss in this subsection the effects of $T_\alpha$, $k_\alpha$, $n_\alpha/ne$ and the type of distribution function always starting from the standard case shown before of a D-T plasma with $n_\alpha/ne$=1% and $\omega=2\omega_{cD}$ at the center.

The influence of $T_\alpha$ is shown in Fig. 6. In Fig. 6b, we have taken the same bi-quadratic profile for $T_\alpha$ as for the other species. We see that the power absorbed by the alphas is not at all proportional to $T_\alpha$, confirming the fact that the width of the cyclotron resonance is not the main factor, for $k_z$ not too small. In both cases, there is a small interval where $P_\alpha$ is larger than $P_D$, which is around 1MeV for the homogeneous profile and 0.3MeV for an inhomogeneous one. These intervals correspond to parameters such that $k_\perp\rho_\alpha$ is of the order of 1 in the outer part of the plasma. In order to understand this feature, let us go back to the power absorption formula. If we assume a plane wave for $\mathbf{E}_\perp$ and neglect $E_z$, as $|E_z| << |\mathbf{E}_\perp|$ in all our cases, $P_L(x)$ is proportional to the following expression, changing x" to $y = k_x(x"-x)/\cos\theta$:

$$P_L(x) = \int_0^{\frac{\pi}{2}} d\theta \int dy \, \frac{n_\sigma q_\sigma^2}{4\sqrt{\pi}\, m_\sigma} \, \frac{e^{-\xi_{n\sigma}^2}}{|k_z| v_{T\sigma}} \, \frac{y^3}{2k_x^4 \rho_\sigma^4} \, e^{-\left(\frac{y}{\sqrt{2}\, k_x \rho_\sigma}\right)^2} |E_+ J_{n-1}(y) + E_- J_{n+1}(y)|^2,$$

where $J_n$ is the Bessel function. The second term determines the width of the resonance layer and the last terms give the contribution of the fields modified by a form factor. Note that it is indeed the product $k_x\rho_\sigma$ which enters into this formula. Due to the Bessel function, this form factor is proportional to $(k_x\rho_\sigma)^n$ for small $k_x\rho_\sigma$, inversely proportional to $k_x\rho_\sigma$ for large $k_x\rho_\sigma$ and has a maximum in between. In Fig.7, we have plotted the contribution of $E_x$ to the form factor, as it is the dominant component of the field, which reads:

$$g(k_x \rho_\sigma) = \int dy \, \frac{y^3}{2k_x^4 \rho_\sigma^4} \, e^{-\left(\frac{y}{\sqrt{2}\, k_x \rho_\sigma}\right)^2} |E_{x0} [J_{n-1} + J_{n+1}]|^2$$

$$= |E_{x0}|^2 \int dy \, \frac{2n^2 y}{k_x^4 \rho_\sigma^4} \, e^{-\left(\frac{y}{\sqrt{2}\, k_x \rho_\sigma}\right)^2} J_n^2(y) .$$

Fig.7 shows that the form factor g has a maximum for $k_x\rho_\sigma$ around n/2, which confirms the result obtained previously (Fig.6). For n=2, we have also plotted the expanded formula $g \approx (k_x\rho_\sigma)^2$ (large dots). We clealy see that for $k_x\rho_\sigma \geq 1$, it much overestimates the integral form.

This has another important consequence. It means that the amount of power absorbed between x and x+dx depends directly on the effective value of $\rho_\sigma^2$ around x. Therefore, if we want to approximate a non-Maxwellian distribution function with a Maxwellian, both should have the

same effective $\rho_\sigma^2$, defined as $\rho_\sigma^2 = \langle v_\perp^2 \rangle(x) / 2\omega_{c\sigma}^2$, where the perpendicular velocity squared is averaged over the equilibrium distribution function considered:

$$\langle v_\perp^2 \rangle(\mathbf{x}) = \int d\mathbf{v}\, v_\perp^2\, f_\sigma^{(0)}(\mathbf{x},\mathbf{v}).$$

Note that for a Maxwellian, $\langle v_\perp^2 \rangle(x) = v_{T\sigma}^2(x)$. In order to illustrate this, we have compared the results obtained with a bi-Maxwellian, that is with two alpha species, and with a single Maxwellian. For the bi-Maxwellian, we have taken: $T_{\alpha 1} = 0.4$ MeV, $T_{\alpha 2} = 1.2$ MeV and $n_{\alpha 1}/n_e = n_{\alpha 2}/n_e = 0.5\%$; and for the single Maxwellian: $T_\alpha = 0.8$ MeV and $n_\alpha/n_e = 1\%$. These values have been chosen such that the total alpha density and the effective value of $\rho_\sigma^2$ are the same. The results obtained with SEMAL show that both alpha power absorption profiles are very similar, as well as the total absorbed power. This shows that we can approximate any distribution function using a Maxwellian with $v_{T\sigma}^2(x) = \langle v_\perp^2 \rangle(x)$. In particular, the alphas are expected to have a slowing-down distribution function of the form [10]:

$$f_{slow}^{(0)} = \frac{3}{4\pi \ln\left(1 + \left(\frac{v_0}{v_c}\right)^3\right)} \frac{1}{v^3 + v_c^3} \cdot \gamma(v_0 - v),$$

with $v_c = \left(3\sqrt{\pi}\, \frac{m_\alpha + m_i}{m_\alpha m_i} m_e\right)^{1/3} \left(\frac{T_e}{m_e}\right)^{1/2}$,

and where $\gamma(v_0 - v)$ is the step-function and $v_0 = 1.3 \cdot 10^7 m/s$ is the birth velocity of the alphas. Using the standard parameters and this slowing-down distribution function, we obtain $\langle v_\perp^2 \rangle_{slow} = 3.8 \cdot 10^{13} m^2/s^2$, which corresponds to a Maxwellian with $T_\alpha = 0.8$ MeV. We see that this

equivalent Maxwellian temperature is much smaller than the 3.5MeV of the birth temperature. This has also been found by Koch[10]. He has compared the imaginary part of $K_{xx}$, the first term of the dielectric tensor, obtained with a Maxwellian and the slowing-down distribution function. In Fig.8, we show the equivalent Maxwellian temperature defined by $T_\alpha = m_\alpha \langle v_\perp^2 \rangle_{slow}/2$ versus $T_e$. We see that the "effective" temperature of the alphas varies between 0.3 and 1.4 MeV for $T_e$ between 0.01 and 100 keV.

The effect of $k_z$ on the power absorbed by the different species is shown on Fig. 9 for the standard case ($T_\alpha$=3.5MeV, $n_\alpha/ne$=1%, D-T). We see that $P_\alpha/P_{tot}$ varies only between 20 and 40%, for $k_z$ not too small, but the distribution of the power between electrons, deuterium and tritium changes much more. This is the same with $T_\alpha$ inhomogeneous. Note that for large $k_z$, electron absorption is important. For small $k_z$, $P_D$ is smaller than $P_\alpha$ at the second harmonic, as mentioned in [2]. For $k_z \geq 2 m^{-1}$ ($k_z R_0 \geq 6$), the main effect of $k_z$ is to determine the amount of alpha power absorption near the edge at the highest harmonic.

The concentration $n_\alpha/n_e$ is, of course, the main parameter which determines the degradation of heating due to alphas particles. This is clearly seen in Fig. 10. For a concentration higher than 2%, more than 50% of the power is absorbed by the alphas for the standard case considered. This dramatic effect is mainly due to the enhancement of alpha power absorption at the third harmonic near the edge such that most of the power is absorbed before it reaches the center. Once again, it is not only due to a higher absorption at the second harmonic of alphas compared with the one at the second harmonic of deuterium. As an

example, for $n_\alpha/n_e$=6%, $P_\alpha/P_{tot}$=75% at the third harmonic, but only 15.5% at the second. Moreover, note that in the outer 60cm, already 72% and 5.5% is absorbed by the alphas at the third and second harmonic respectively, that is 77.5% of the total power.

## 4. SUMMARY AND CONCLUSIONS

We have developed a code SEMAL, which solves the linearized Vlasov-Maxwell equations in a 1-D slab inhomogeneous plasma, without any approximation as to the size of the Larmor radii compared with the wavelengths. Furthermore, it is not limited to the second harmonic of the cyclotron frequency. In all the cases considered we have summed the contributions of the harmonic numbers n=-20 through n=+20, but the code is not limited to these values. We have also derived a formula for the local power absorption. This formula is positive-definite and is also valid to all orders in the Larmor radii and for arbitrary inhomogeneous profiles. Our model assumes Maxwellian equilibrium distribution functions, $k_y$=0 in the dielectric response of the plasma, and a slowly varying magnetic field. It leads to solving a system of one first-order and two second-order integro-differential equations for $E_x$ and $E_y$, $E_z$ respectively. The model is non-local in the sense that, due to the integral part of the equations, fields of the whole plasma contribute to the field at one point.

This non-local model is therefore well appropriate for studying the effects of fusion alpha particles on ICRF heating as they have very large Larmor radii. Nevertheless, we have not considered the $1/v^3$ dependence of the alpha distribution function in order to be able to invert the Fourier transform of the equations. However, we have shown that the effective $\rho_\alpha^2$

is one of the main parameters which influences the power absorbed by the particles. Therefore, the approximation of the slowing-down distribution function by a Maxwellian having the same average perpendicular velocity, $\langle v_\perp^2 \rangle$, should reproduce the main effect on ICRF heating. We have shown that this equivalent Maxwellian temperature, $T_\alpha = m_\alpha \langle v_\perp^2 \rangle / 2$, varies between 0.3 and 1.4MeV for a wide range of different slowing-down distribution functions. This was also found by comparing the dielectric tensor obtained with a slowing-down and a Maxwellian distribution function [9].

We have shown in subsection III.1 that the power absorbed by alphas at some harmonic is much less important, compared with the power absorbed by deuterium at the same harmonic, than what one would expect from the local model, for $k_\perp \rho_\alpha > 1$. This explains why the local model considerably overestimates the alpha power absorption. Even for a small alpha concentration ($n_\alpha/ne < 1\%$) the difference is significant because, with the local model, the wave cannot reach the cyclotron resonance at the center as it is completely damped by the alphas before.

Another important feature which has to be taken into account is higher-harmonic heating. Indeed, even if the scenario considered is tuned to the second harmonic of $\omega_{cD}$, the frequency at the edge of the plasma will be close to the next harmonic. As the alphas' cyclotron resonance layer is very broad, they will absorb a lot of energy near the edge at this higher harmonic. Note that this effect will be even more important in larger devices or for heating scenarii at higher frequencies, as has be seen in Sec.III.1. We have also shown that for an alpha

concentration larger than 2%, for the standard scenario considered, most of the power was absorbed by the alphas near the edge.

We have also found, by varying $T_\alpha$ as well as the profile of $T_\alpha$, that the absorbed power is enhanced if $k_\perp\rho_\alpha$ is of the order of 1 for the second harmonic. A simple study of the structure of $P_L(x)$ shows that it is proportional to a form factor which is maximum at $k_\perp\rho_\alpha \approx n/2$. However, this constraint cannot easily be avoided as the profile of $T_\alpha$ will probably be fixed by the experiment and transport conditions. Therefore one would have to move the cyclotron resonance in a region such that $k_\perp\rho_\alpha<n/4$ or even better $k_\perp\rho_\alpha>3n/2$, while still heating the bulk plasma. Nevertheless, one may at least avoid that $k_\perp\rho_\alpha \sim n/2$ near the edge, if alpha power absorption occurs there.

This study indicates that an important parameter is the effective Larmor radius, which is directly related to the perpendicular velocity squared, $\langle v_\perp^2 \rangle$, averaged over the equilibrium distribution function considered. Therefore, a Maxwellian distribution function with $v_{T_\perp\alpha}^2 = \langle v_\perp^2 \rangle_{slow}$, where $\langle v_\perp^2 \rangle_{slow}$ is averaged over the slowing-down distribution function, should reproduce well the effect of alphas on ICRF heating.

We have shown that $P_\alpha/P_{tot}$ is not very sensitive to the value of $k_z$ for not too a small alpha concentration. Nevertheless, one can avoid the edge alpha heating by lowering the value of $k_z$, that is by narrowing the cyclotron resonance layer. However, in JET, $k_z$ has a typical value between 5 and 10 $m^{-1}$ (toroidal N=15-30) which enhances the alpha heating in the outer part of the plasma.

The main parameter is, of course, the alpha particle concentration. We have seen that, eventhough the alphas absorb much less power than expected from local models, they have a very strong influence for $n_\alpha/n_e>2\%$. This is mainly due to the edge alpha heating at the third and also at the second harmonics. However, the density profile may be more peaked than that of the other species, as they are created in the center. This would then decrease the alpha concentration near the edge and greatly improve the heating scenario.

Finally, the key issues to reduce the effects of alpha particles on second-harmonic heating are:

1) avoid $k_\perp\rho_\alpha \approx n/2$ in the outer part of the plasma,

2) maximize the edge value of $|\xi_{n\alpha}|$ at the closest harmonic n.

Note that the second constraint can be satisfied either by changing $k_z$ or the frequency $\omega$, if $k_z$ is not too large. However the first constraint, which is the most important one, is difficult to fulfill for an effective alpha temperature around 1MeV. Indeed, if we introduce the simplified dispersion relation for the fast wave, $k_\perp \approx k=\omega/c_A$, $T_\alpha$=0.8MeV, 50-50 D-T plasma with $n_e=10^{20}m^{-3}$, we obtain:

$$k_\perp \rho_\alpha \cong \frac{\omega}{\omega_{c\alpha}} \frac{v_{T\alpha}}{2 c_A} \cong \frac{\omega}{\omega_{c\alpha}} \frac{2.25}{B_0} \quad .$$

For second-harmonic heating and most of large tokamaks, $\omega \approx 2.5\omega_{c\alpha}$ in the outer part of the plasma, which gives for $B_0 \approx 4T$, $k_\perp\rho_\alpha \approx 1.4$. This value is close to n/2 for both the second and third harmonic and there are not many parameters free to modify it. Therefore, we expect an efficient alpha

heating near the edge and thus a strong degradation of deuterium heating, except if the alpha density profile is more peaked than that of the other species, such that the edge alpha concentration is smaller or equal to 1%.

## ACKNOWLEDGMENTS

The authors would like to thank Dr. T. Hellsten for useful comments. Drs. K. Appert and F. Skiff are also acknowledged for many stimulating discussions.

This work was partly supported by the Swiss National Science Foundation.

## REFERENCES

[1] HELLSTEN, T., APPERT, K., VACLAVIK, J., VILLARD, L., Nucl. Fusion **25** (1985) 99.

[2] KAY, A., CAIRNS, R.A., LASHMORE-DAVIES, C.N., Plasma Phys. & Contr. Fusion, **30** (1988) 471.

[3] VAN EESTER, D., KOCH, R., NYS, V., in Theory of Fusion Plasmas (Proc. Joint Varenna-Lausanne Int. Workshop, Varenna, 1990), Editrice Compositori, Bologna (1990) 339.

[4] SAUTER, O., VACLAVIK, J., in Theory of Fusion Plasmas (Proc. Joint Varenna-Lausanne Int. Workshop, Varenna, 1990), Editrice Compositori, Bologna (1990) 403.

[5] SAUTER, O., VACLAVIK, J., SKIFF, F., Phys. Fluids B **2** (1990) 475.

[6] FRIED, B.D., CONTE, S.D., The Plasma Dispersion Function, Academic, New York, NY (1961).

[7] LLOBET, X., APPERT, K., BONDESON, A., VACLAVIK, J., Comput. Phys. Commun. **59** (1990) 199.

[8] JAUN, A., VACLAVIK, J., in Theory of Fusion Plasmas (Proc. Joint Varenna-Lausanne Int. Workshop, Varenna, 1990), Editrice Compositori, Bologna (1990) 461.

[9] APPERT, K., HELLSTEN, T., LUETJENS, H., SAUTER, O., VACLAVIK, J., VILLARD, L., in Proc. 7th Int. Conf. on Plasma Physics, Kiev, Invited Papers, **2** (1987) 1230.

[10] KOCH, R., Phys. Lett. A **157** (1991) 399.

FIGURE CAPTIONS

Figure 1: Full hot-plasma dispersion relation for the standard parameters with $n_\alpha/n_e=1\%$ and homogeneous alpha temperature profile. At x=0, $\omega=2\omega_{cD}$ and at x=1m, $\omega=4\omega_{cT}$.

Figure 2: $\bar{P}_L(x)$, for the standard parameters with $n_\alpha/n_e=0,0.1$ and 1%. a) Local model (ISMENE). b) Non-local model (SEMAL).

Figure 3: Real part of $E_x$ for the cases shown in Fig.2 with $n_\alpha/n_e=1\%$ (dotted line).

Figure 4: $\bar{P}_L(x)$ for 4 scenarii with $n_\alpha/n_e=1\%$: $\omega=2\omega_{cH}$, $\omega=2\omega_c{}^3He$, $\omega=2\omega_{cT}$, $\omega=2\omega_{cD}$. 20% of H or $^3He$ has been added in the first two scenarii.a) ISMENE; b) SEMAL.

Figure 5: 4th, 5th, 6th harmonics' and total power absorption density $P_{L\alpha}(x)$ of alpha particles for the case with hydrogen, Fig.4b.

Figure 6: $\bar{P}_{L\sigma}(x_{pl})$, divided by the total power $\bar{P}_L(x_{pl})$, where $x_{pl}$ is the left hand-side boundary of the plasma, for different central values of $T_\alpha$ with $k_z=5m^{-1}$ and $n_\alpha/n_e=1\%$. The alpha temperature profile is constant (a) or bi-quadratic (b).

Figure 7: Form factor $g(k_x\rho_\sigma)$ for harmonic numbers n=1,2,3,4 and 7. For n=2, g expanded to second order in $k_x\rho_\sigma$ is plotted (large dots).

Figure 8: Equivalent Maxwellian temperature, for the slowing-down distribution function considered, calculated such that $v_{T\alpha}^2 = \langle v_\perp^2 \rangle_{slow}$.

Figure 9: The same plot as in Fig. 6, but for different values of $k_z$, with $T_\alpha$=3.5MeV and $n_\alpha/n_e$=1%. a) homogeneous and b) inhomogeneous $T_\alpha$ profile.

Figure 10: The same plot as in Fig. 6, but for different values of $n_\alpha/n_e$, with $T_\alpha$=3.5MeV and $k_z=5m^{-1}$. Only the case with an inhomogeneous $T_\alpha$ profile is shown, as the results are very similar for the homogeneous case.

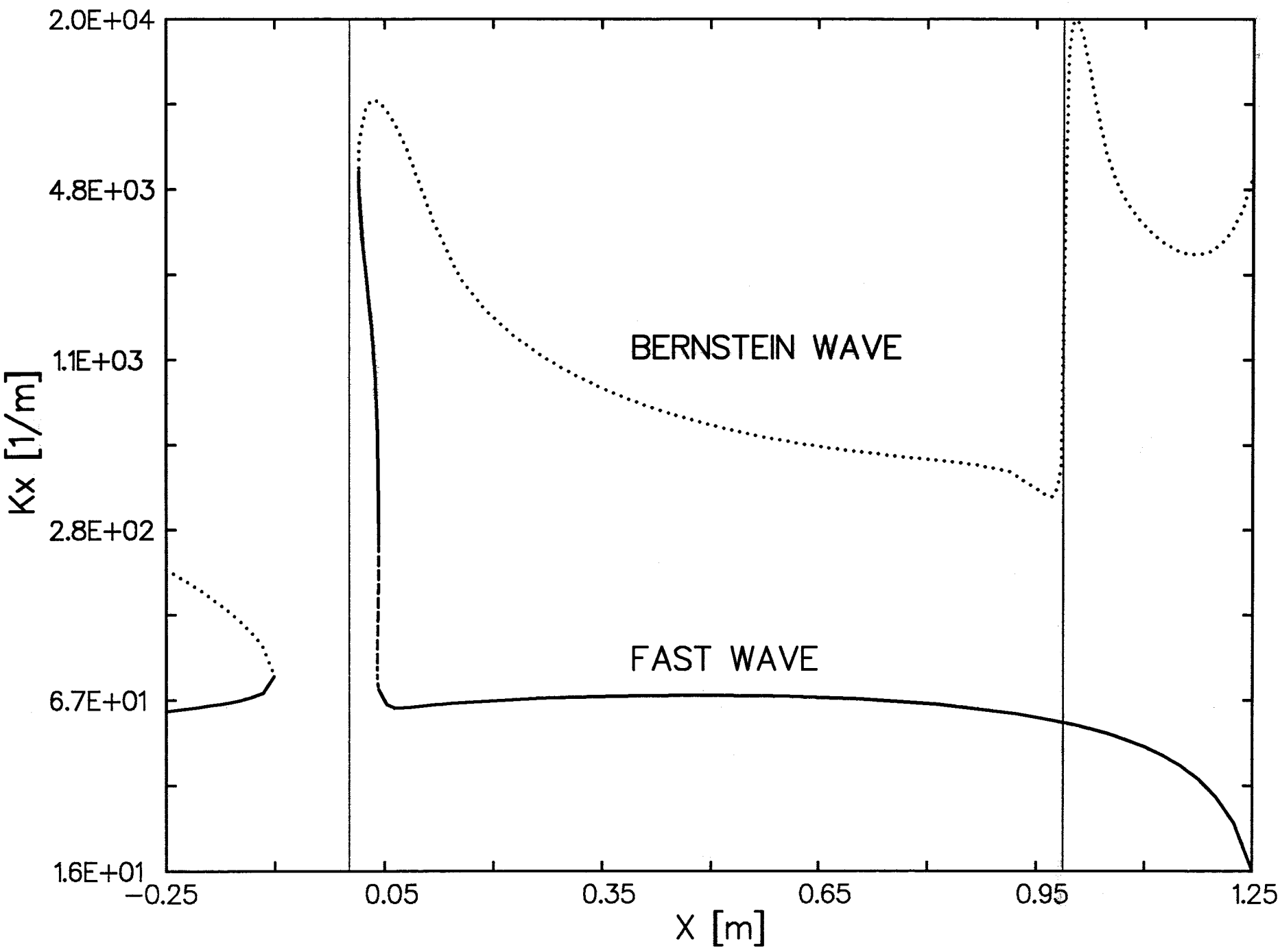
2.0E+04
4.8E+03
1.1E+03
2.8E+02
6.7E+01
1.6E+01
Kx [1/m]
BERNSTEIN WAVE
FAST WAVE
−0.25
0.05
0.35
0.65
0.95
1.25
X [m]

Fig. 1

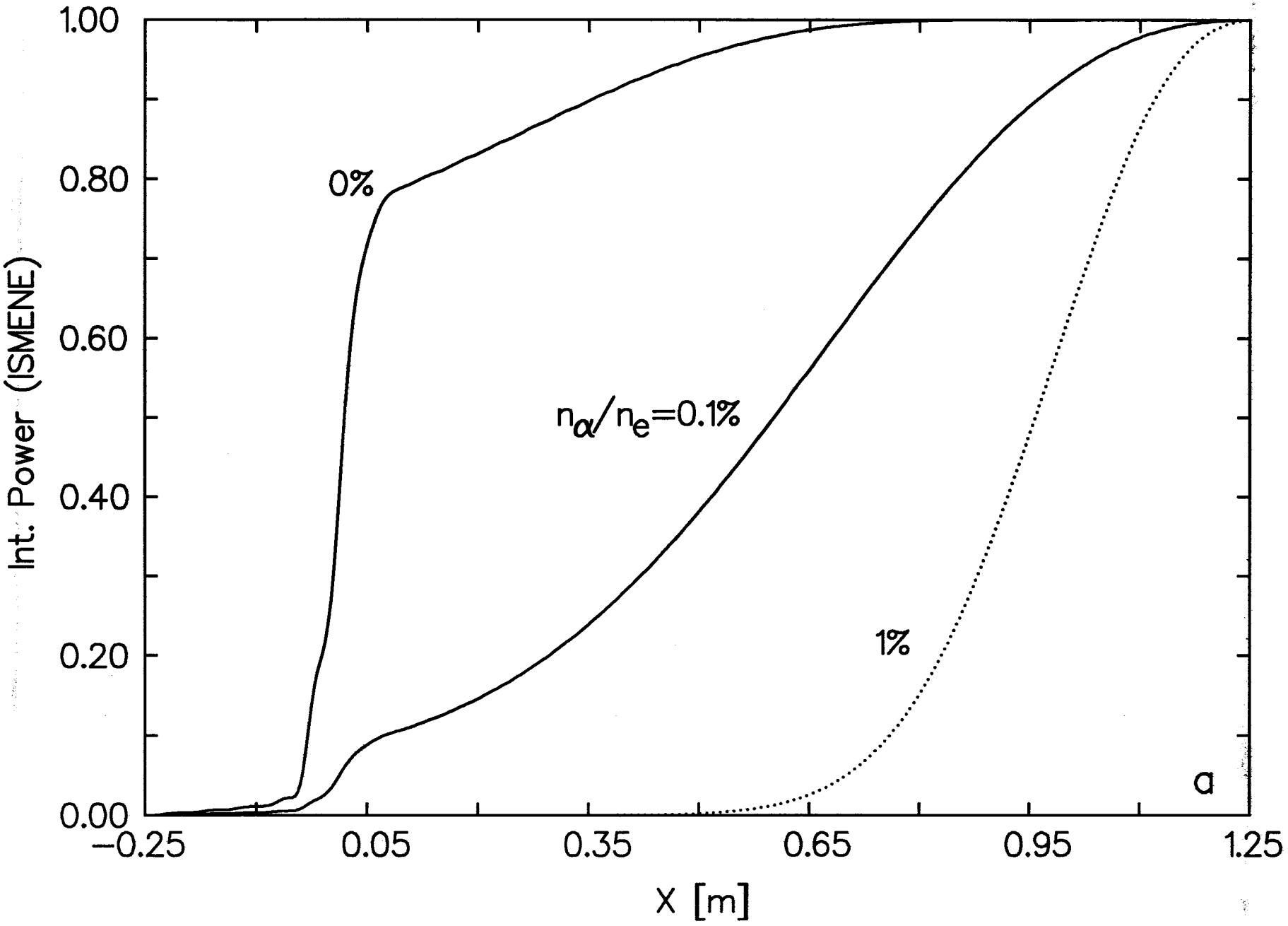
1.00
0.80
0.60
0.40
0.20
0.00
Int. Power (ISMENE)
0%
$n_\alpha/n_e$=0.1%
1%
a
−0.25
0.05
0.35
0.65
0.95
1.25
X [m]

Fig. 2a

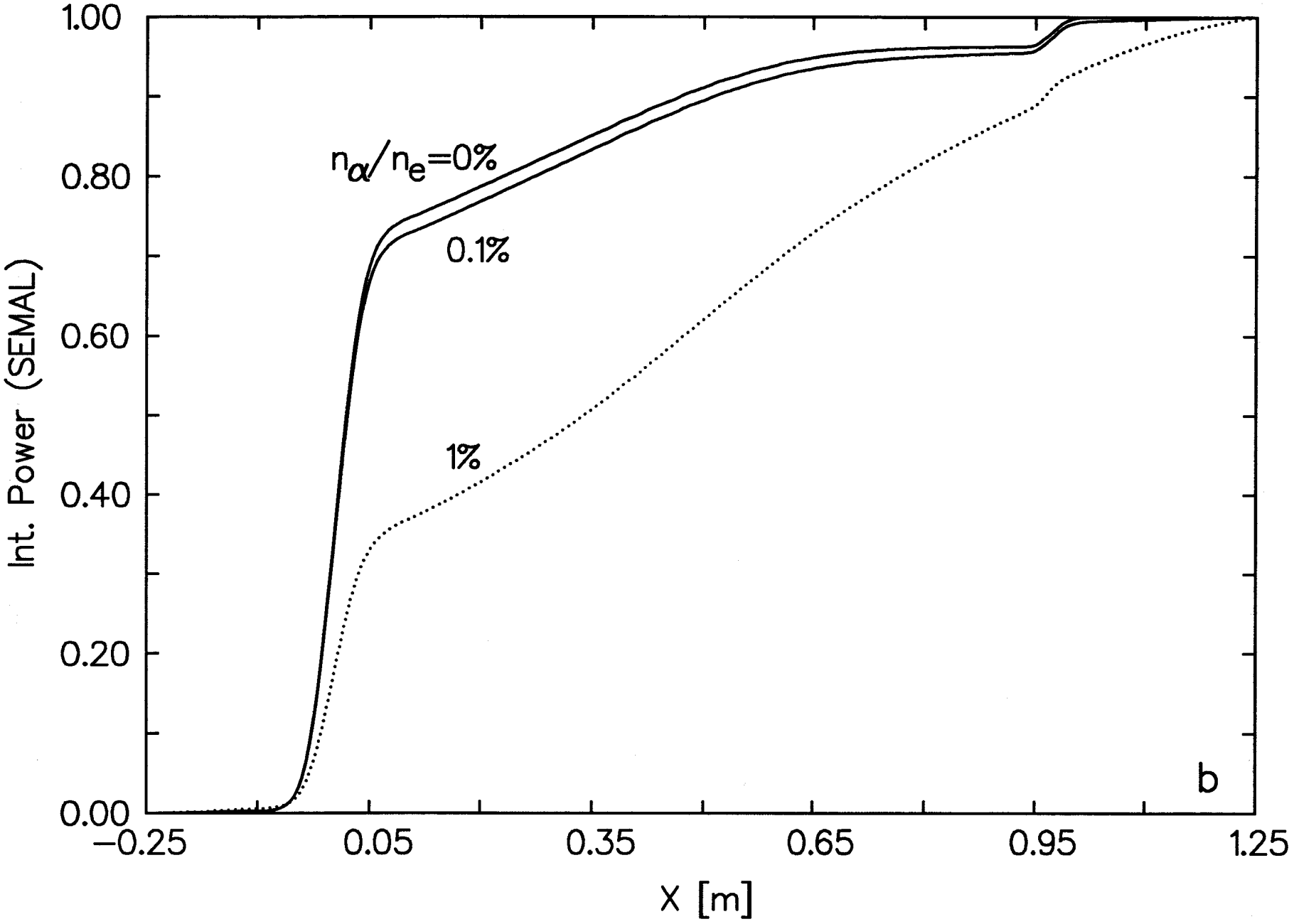
1.00
0.80
0.60
0.40
0.20
0.00
Int. Power (SEMAL)
$n_\alpha/n_e$=0%
0.1%
1%
b
−0.25
0.05
0.35
0.65
0.95
1.25
X [m]

Fig. 2b

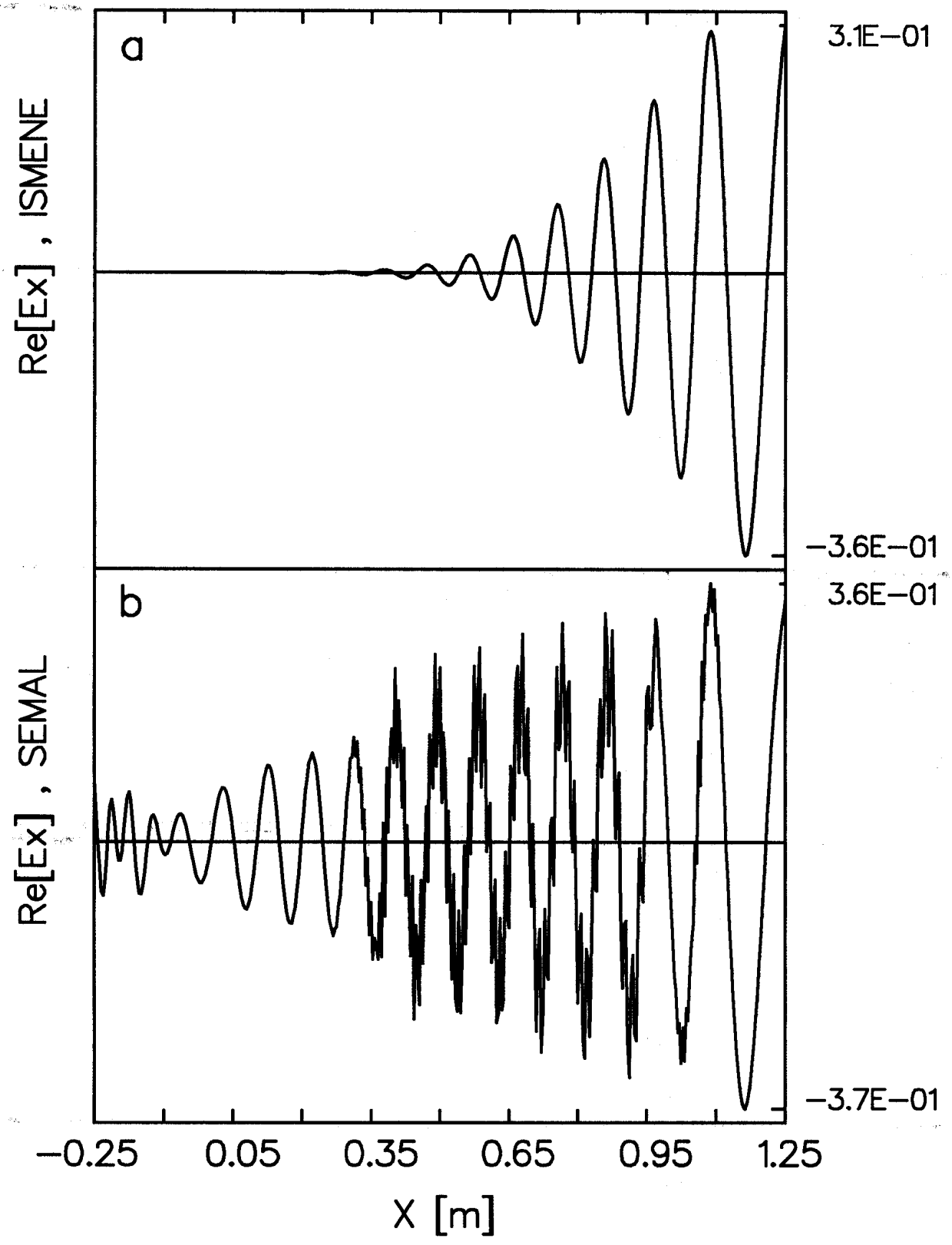
a
b
3.1E−01
−3.6E−01
3.6E−01
−3.7E−01
Re[Ex] , ISMENE
Re[Ex] , SEMAL
−0.25
0.05
0.35
0.65
0.95
1.25
X [m]

Fig. 3

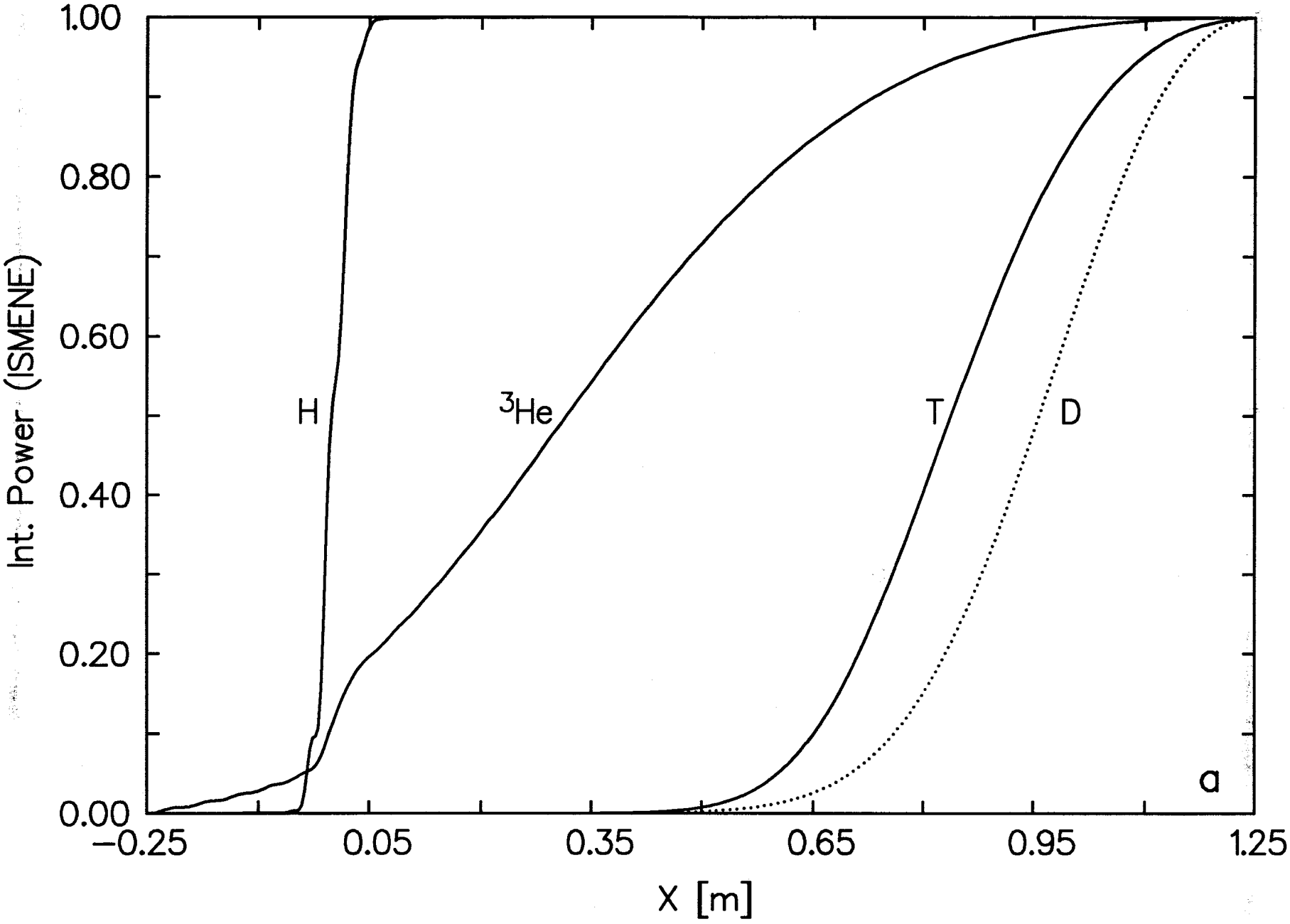
1.00
0.80
0.60
0.40
0.20
0.00
Int. Power (ISMENE)
H
3He
T
D
a
−0.25
0.05
0.35
0.65
0.95
1.25
X [m]

Fig. 4a

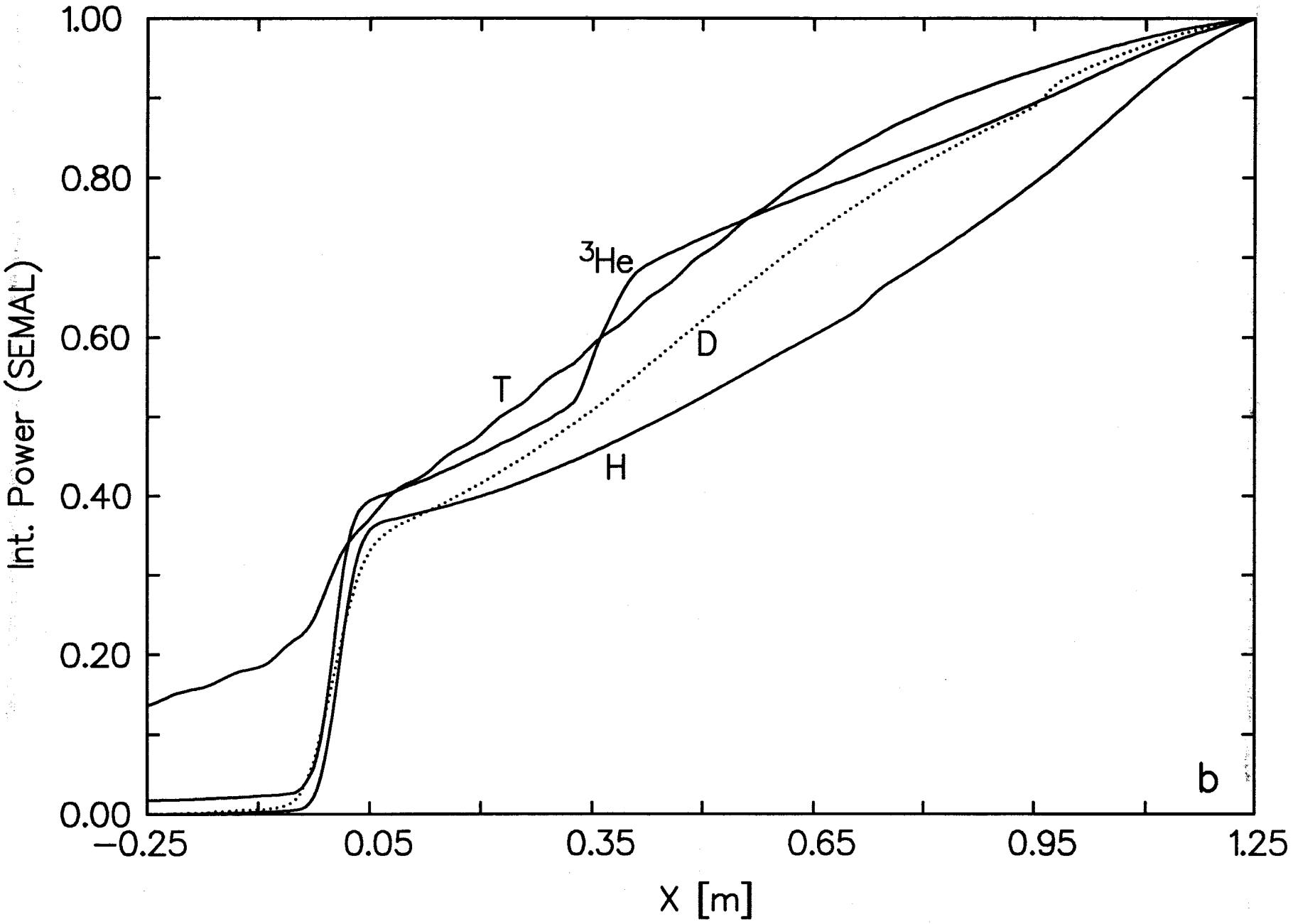
1.00
0.80
0.60
0.40
0.20
0.00
Int. Power (SEMAL)
−0.25
0.05
0.35
0.65
0.95
1.25
X [m]
$^3$He
T
D
H
b

Fig. 4b

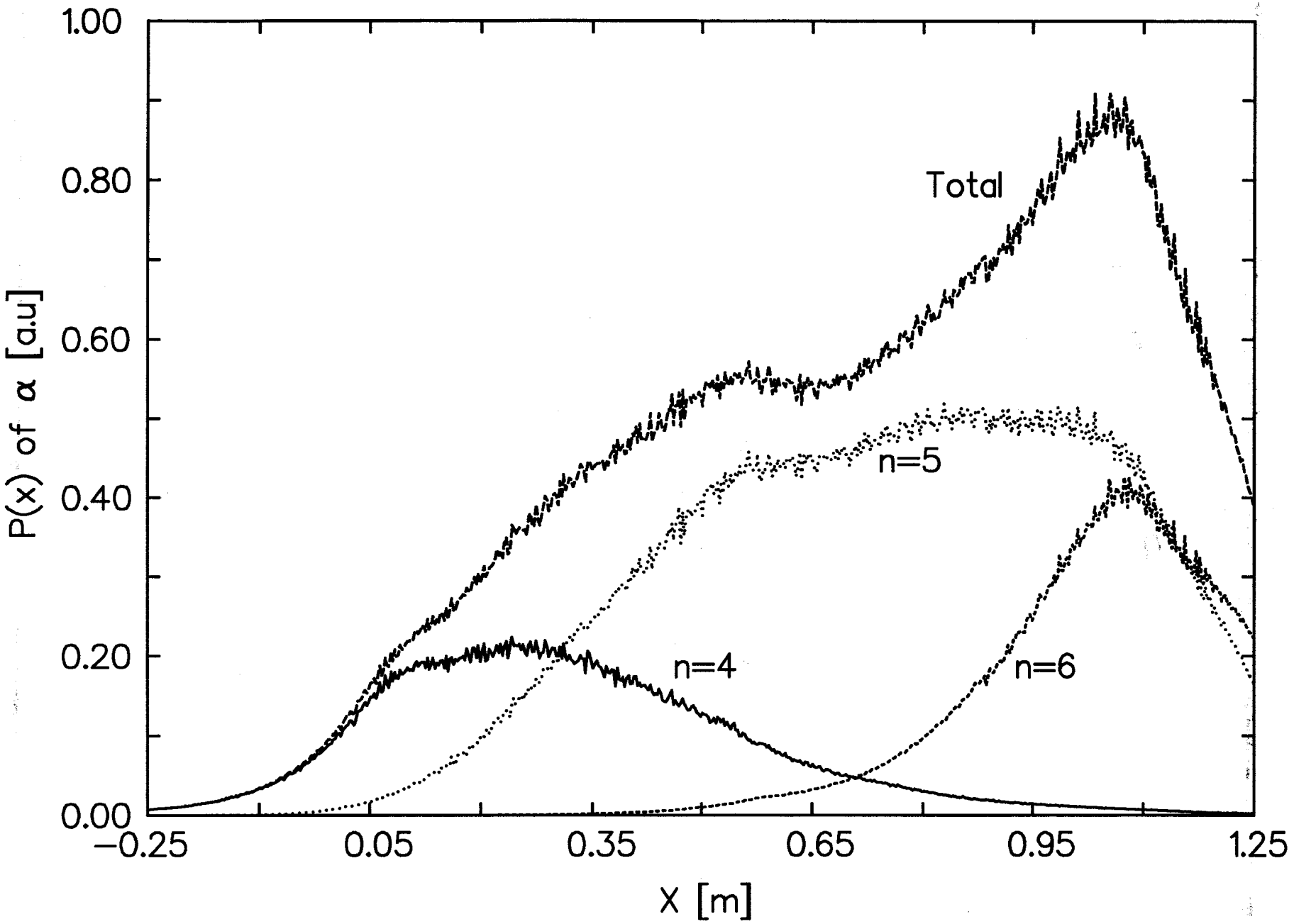
1.00
0.80
0.60
0.40
0.20
0.00
P(x) of α [a.u]
Total
n=5
n=4
n=6
−0.25
0.05
0.35
0.65
0.95
1.25
X [m]

Fig. 5

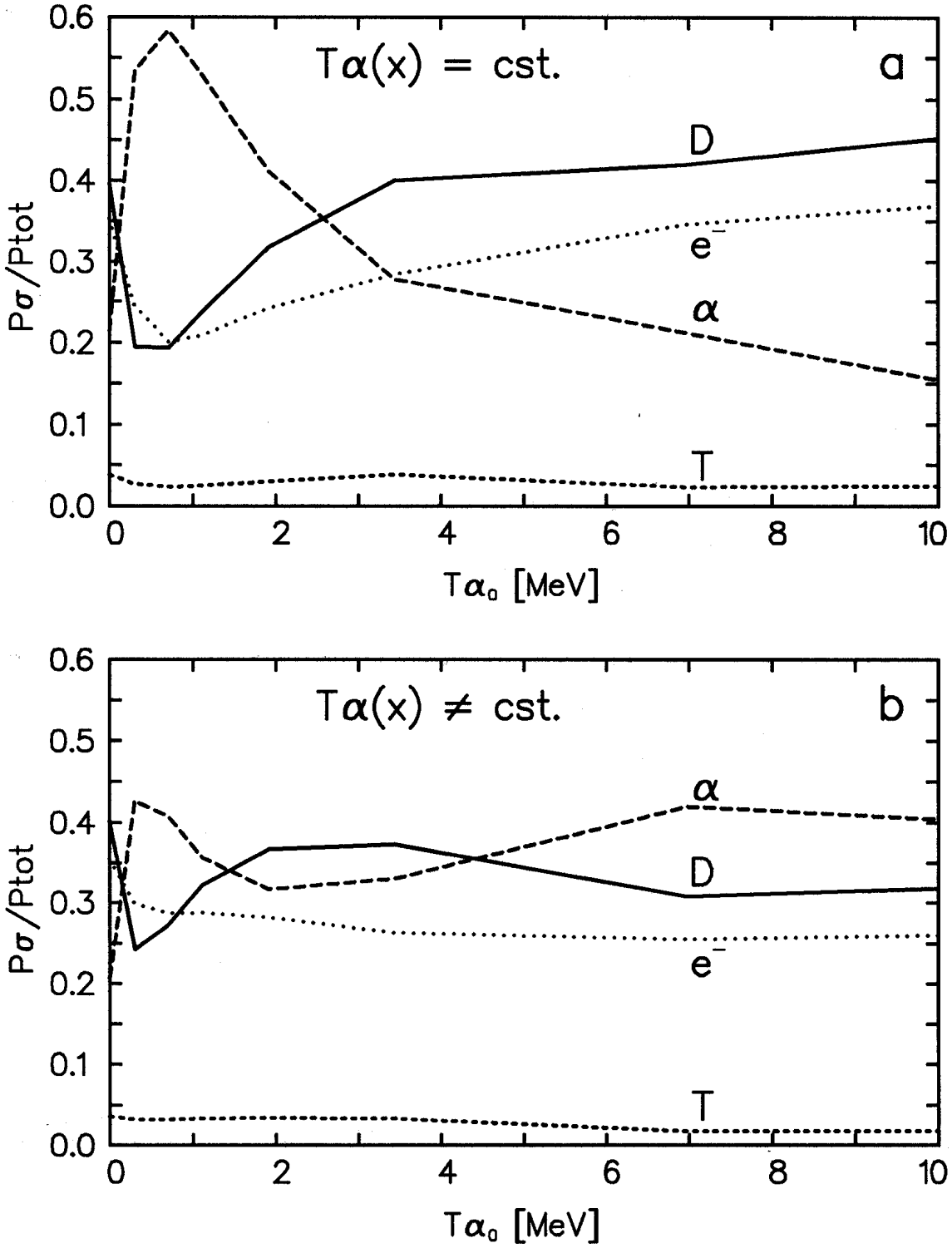


Fig. 6

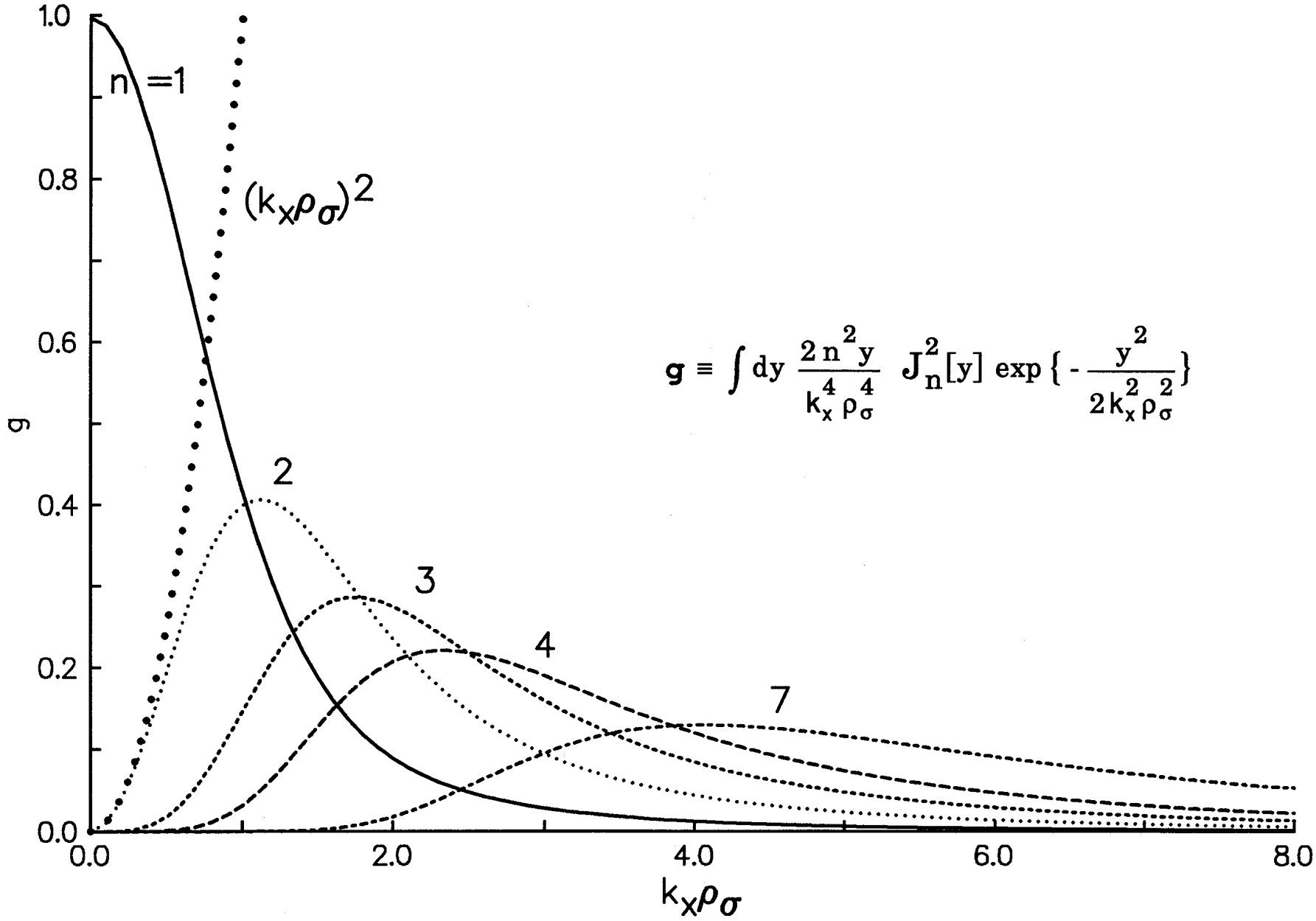
1.0
0.8
0.6
0.4
0.2
0.0
g
n =1
$(k_x\rho_\sigma)^2$
2
3
4
7
$g \equiv \int dy \frac{2n^2y}{k_x^4\rho_\sigma^4} J_n^2[y] \exp\{-\frac{y^2}{2k_x^2\rho_\sigma^2}\}$
0.0
2.0
4.0
6.0
8.0
$k_x\rho_\sigma$

Fig. 7

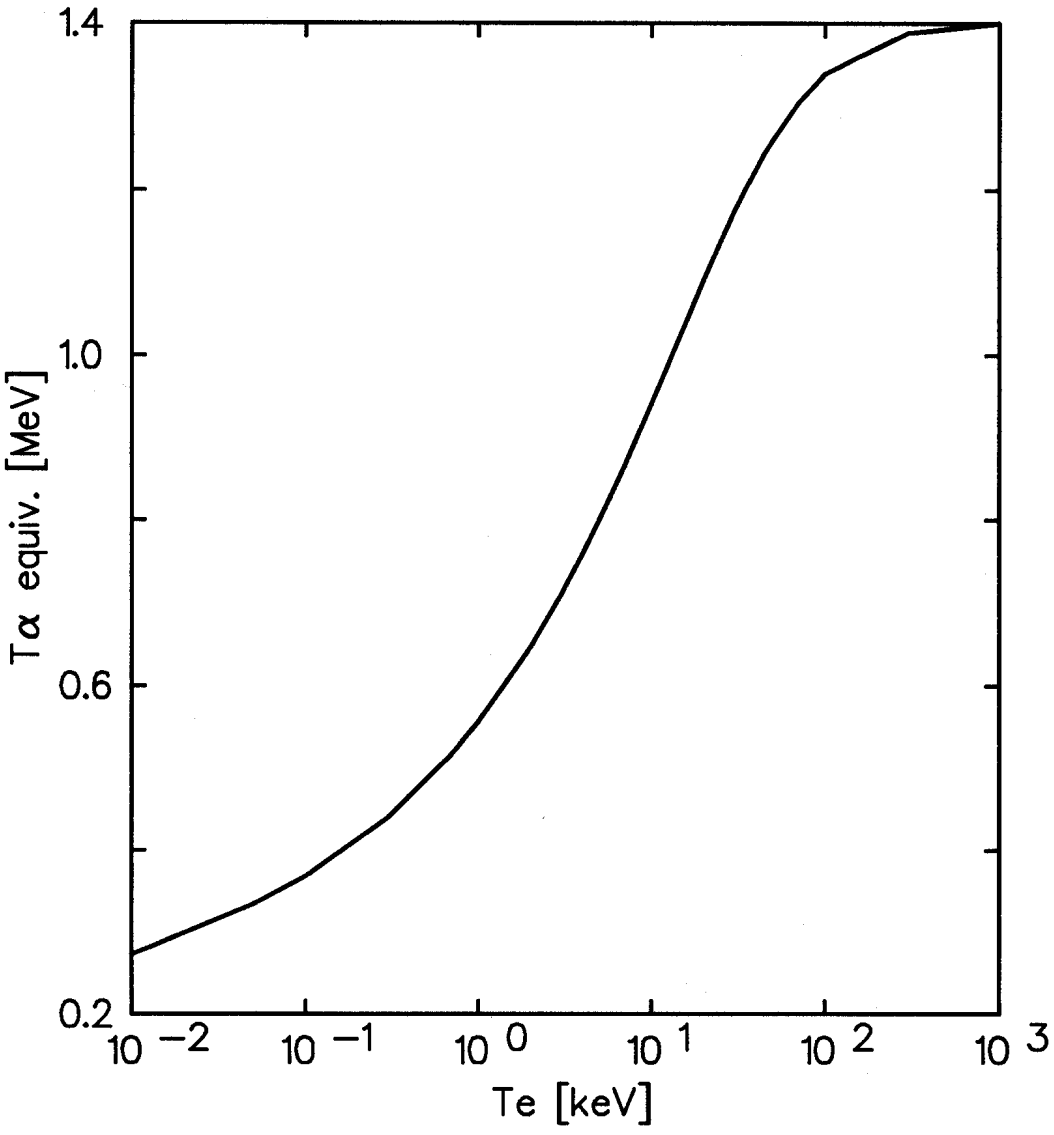


Fig. 8

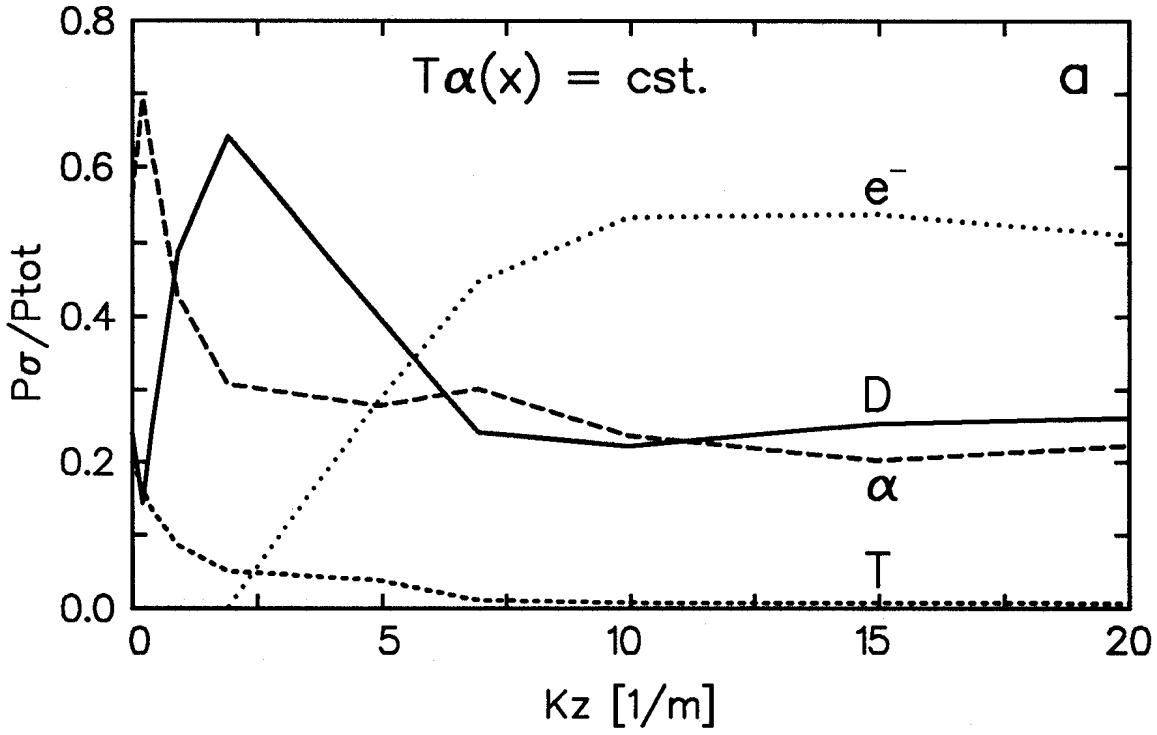
Tα(x) = cst.
a
e⁻
D
α
T
Pσ/Ptot
Kz [1/m]
0.0
0.2
0.4
0.6
0.8
0
5
10
15
20

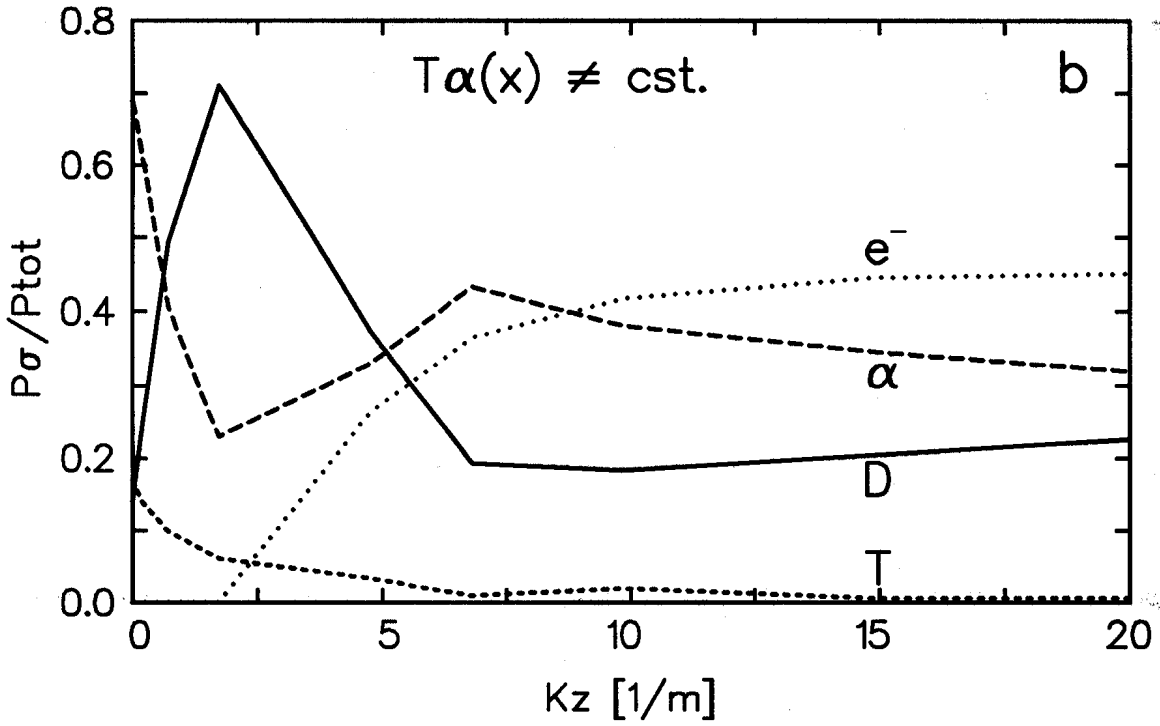
Tα(x) ≠ cst.
b
e⁻
α
D
T
Pσ/Ptot
Kz [1/m]
0.0
0.2
0.4
0.6
0.8
0
5
10
15
20

Fig. 9

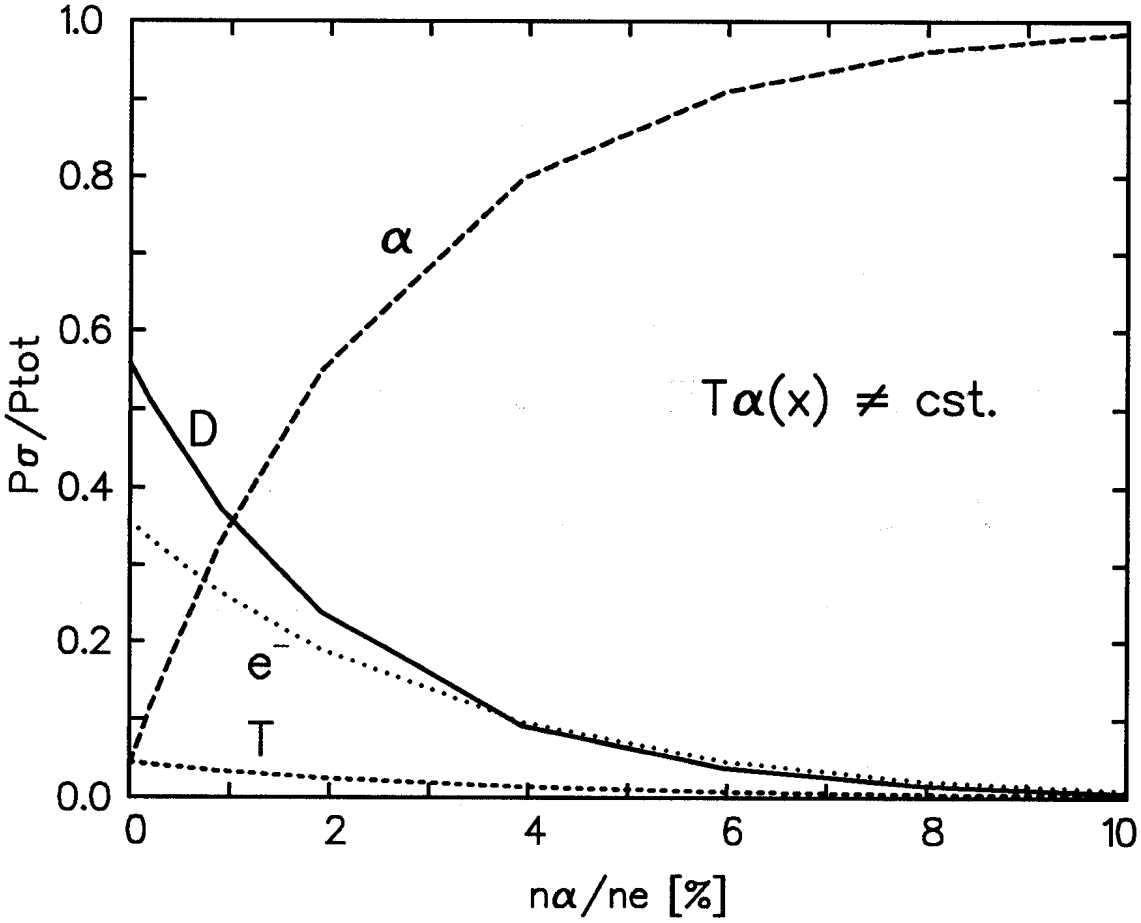


Fig. 10